Structural Inhibition of Silver Surface Oxidation

Marie E. Turano,[†] Ludo B. F. Juurlink,[‡] Maxwell Z. Gillum,[†] Elizabeth A. Jamka,[†] and Daniel R. Killelea[*,†]

[†]*Department of Chemistry and Biochemistry, Loyola University Chicago, 1068 W. Sheridan Road, Chicago, Illinois 60660, United States*

[‡]*Leiden Institute of Chemistry, Leiden University, PO Box 9502, 2300 RA Leiden, The Netherlands*

E-mail: dkillelea@luc.edu

Phone: (773) 508 3136

Abstract

Surface structure and oxidation are key to silver-based heterogeneous catalysis. Prevention of surface reconstruction may favor electrophilic oxygen, which is believed to be the active species in silver-catalyzed oxidation. To determine whether terrace width or step geometry enables control of oxidation and concomitant reconstruction, we investigated oxidation of the topmost layer of a curved Ag(111) crystal. This crystal contains a range of terrace widths having either A or B-type step geometries. Atomic oxygen was used to facilitate oxidation, Temperature Programmed Desorption quantified the extent of oxygen adsorption, and Scanning Tunneling Microscopy characterized formation of reconstructed areas. While A-type steps prove to have little influence, B-type steps hinder reconstruction. We attribute the difference to geometric-dependent growth mechanisms of silver oxide surface reconstructions.

Introduction

Since the 1970's, significant effort has gone into the characterization of oxidized silver (Ag) surfaces to determine the oxygen species present and their chemical behavior.[1–6] This effort is largely motivated by the industrial relevance of partial oxidation reactions over silver catalysts, particularly the industrial transformation of ethylene to ethylene oxide and methanol to formaldehyde at temperatures above 500 K.[7–11] While consensus has emerged regarding many details of the mechanisms for these reactions,[12–15] the exact nature of the reactive oxygenaceous species is still under debate. In particular, the importance of surface reconstructions and defects are active areas of research, where the goal is to use an atomic-level understanding to further develop the heterogeneously catalyzed chemistry of silver.[11,14,16–21]

Different oxygenaceous phases may form on silver surfaces depending on the conditions, and several have been characterized using a combination of experimental and theoretical methods.[1,6,11,16,22–24] These reconstructions reflect different atomic arrangements and amounts of oxygen incorporation. Although oxygen in the reconstructions is reactive, the reconstructions are comprised of nucleophilic oxygen, which is attributed to formation of combustion products. The electrophilic oxygen thought to be responsible for the partial oxidation of ethylene under industrial catalytic conditions is not expected to be present in the reconstructions.[17,24,25] Because this potentially enhances the amount of catalytically active oxygen present on the surface, it is interesting to mitigate the formation of the reconstructions.

Shape control may aid in optimizing catalytic activity of Ag particles for various reasons[26,27] and could mitigate formation of reconstructions. It is known that the atomic arrangements of flat terraces influence the surface reactivity of silver.[28,29] For example, Ag(100) surfaces do not undergo the extensive oxygen-induced reconstructions that occur on Ag(111).[30,31] Beyond the atomic arrangement of terraces, there is also an emerging understanding of the subtle role of step geometry on the reactivity of catalytic surfaces.[32–34] Savio et al. used molecular beams to show that O_2 dissociation and subsequent subsurface

oxygen (O_{sub}) formation on Ag were facilitated by open step geometries.[35] However, their studies mostly used surfaces with a (100) terrace structure,[36] rather than the low-energy (111) facets generally proffered by small particles of fcc metals in catalytic applications. Finally, oxygen-induced surface reconstructions on Ag(111) planes, such as the $p(4 \times 4)$ or $p(4 \times 5\ \sqrt{3}\ )$ reconstructions, consist of multiple unit cells and require a significant local adsorbed oxygen (O_{ad}) concentration.[10,11,23] Narrow terraces on small particles may not be able to host such reconstructions and thus, show more resilience towards oxidation. To guide intelligent shape control and improve catalyst performance, our study aims to improve understanding of the influence of common close-packed defect (step) types and terrace types prone to reconstruction.

Curved single crystal surfaces provide a powerful approach for connecting chemical reactivity to step density and geometry.[31,37–40] The curved surfaces expose a systematic range of step defect densities where the step geometry and terrace widths are indexed by the position across the face of the curved single crystal surface. Auras and Juurlink recently reviewed the advances in the applications of such crystals in surface science and catalysis.[41] While many different metallic and more recently, metal oxide materials have been used, curved Ag surfaces appeared in only three studies thus far.[42–44] Crystals with a (111) apex separating sides containing A and B-type steps[42–44] and a symmetric crystal with a (100) apex and A' type steps[42] both predominantly exhibited the expected variation in step density across the crystal. Beyond the very subtle difference in reversible water adsorption to these terraces and steps,[42,43] there have been no reports of the chemical reactivity of curved Ag surfaces.

In this paper, we report results from an investigation of atomic oxygen adsorption on a curved Ag(111) single crystal surface with two types of close-packed steps, A-type and B-type. The crystal shape, size, and orientation are specified in the notation of Auras and Juurlink as c-Ag(111)$[1\bar{1}0]$R31°.[41] A-type steps are characterized by a square arrangement of atoms along the step facet while B-type steps have a triangular arrangement of atoms.[41] We show that the extent of surface reconstructions of the (111) terraces was dependent

on the terrace width and step geometry. Formation of oxygen-induced reconstruction was strongly hindered on the side containing B-type geometry steps, yet reconstruction proceeded readily at the (111) apex and on the A-type step side. Additionally, on A-type stepped surfaces, we found extensive planarization. These findings impact the expected behavior of Ag nanoparticles under oxidizing conditions and present a means of potentially tailoring their catalytic behavior.

Experimental

Experiments were performed in an ultra-high vacuum scanning tunneling microscope (UHV-STM) system described previously.[45] The system consists of two interconnected chambers, a preparation chamber (base pressure of 1×10^{-10} Torr) and an STM chamber (base pressure of 4×10^{-11} Torr). The preparation chamber was equipped with a Specs ErLEED 150 with 3000D controller (LEED), a PHI 10–155 Auger Electron Spectrometer (AES), and a Hiden HAL 3F 301 RC quadrupole mass spectrometer (QMS) for temperature programmed desorption (TPD) analysis. The curved Ag(111) crystal (c-Ag(111)) was obtained from Surface Preparation Labs (Zaandam, NL) and was described in detail in a previous publication.[42] The 8 mm long c-Ag(111) was cut at a 31° angle from a circular cylindrical crystal and polished to expose the (111) surface at the apex, the (110) steps or B-type steps on one side (+ x direction), and the (100) or A-type steps on the other side (- x direction). The STM tip had a range of ± 2.5 mm from the crystal apex at an imaging temperature of ≈ 35 K, which allowed for imaging from about 3 mm off the apex in the B-type step direction to about 2 mm off the apex in the A-type step direction. We focused on the region between 1–2 mm from the apex on both sides of the crystal in this report. The crystal was cleaned using established procedures,[42,43] and cleanliness was verified with LEED and STM. Atomic oxygen was generated by backfilling the preparation chamber with O_2 ($P = 5 \times 10^{-7}$ Torr) that was thermally cracked over a hot Ir filament positioned about 1 - 2 mm from the front face of

the crystal.[16,46] The atomic oxygen exposure across the crystal face was uniform and normal to the top (111) facet; the curvature resulted in only modest attenuation of the O-atom flux towards the edges of the crystal and was the same on both sides. In between atomic oxygen doses, the crystal surface was restored by sputtering and annealing. The STM chamber housed a Pan Style RHK Scanning Tunneling Microscope with a closed cycle helium cryostat that reached a base temperature of 30 K or below. All images were taken at 35 K. STM tips were fashioned using the cut and pull technique from 0.25 mm diameter $Pt_{0.8}Ir_{0.2}$ wire. All images were recorded in constant current mode and were processed using the Gwyddion software package (available at http://gwyddion.net). The images used were processed minimally (e.g., cropping, mean plane subtraction or three-point plane subtraction, and/or removal of streaks or blemishes). Line profiling was done on uncorrected STM images for determination of chemisorbed oxygen coverage (O_c), terrace width, and step density.

Results and Discussion

In order to determine whether O-induced reconstructions of the Ag(111) plane are hindered by particular types of steps or the width of terraces, we used STM to image the surface after various atomic oxygen (AO) exposures to determine structural changes to the surface. Prior to oxidation, though, we imaged and characterized the clean *c*-Ag(111) surface to provide a structural reference. Figure 1 shows representative STM images of the clean surface at 1.0 mm, 1.5 mm, and 2.0 mm from the apex in both the A-type (left column, color coding in blue) and B-type (right column, color coding in red) step directions. The images show regularly spaced steps with predominantly straight step edges. We observed neither significant levels of impurities nor step bunching and/or merging. Some step bunching on the far edges of the clean crystal was found,[42] but these regions were not relevant to the study herein. Step densities, ρ_{step}, were calculated from line profiles taken normal to the step directions. We used the downhill direction scan after confirming that the uphill direction scan yielded

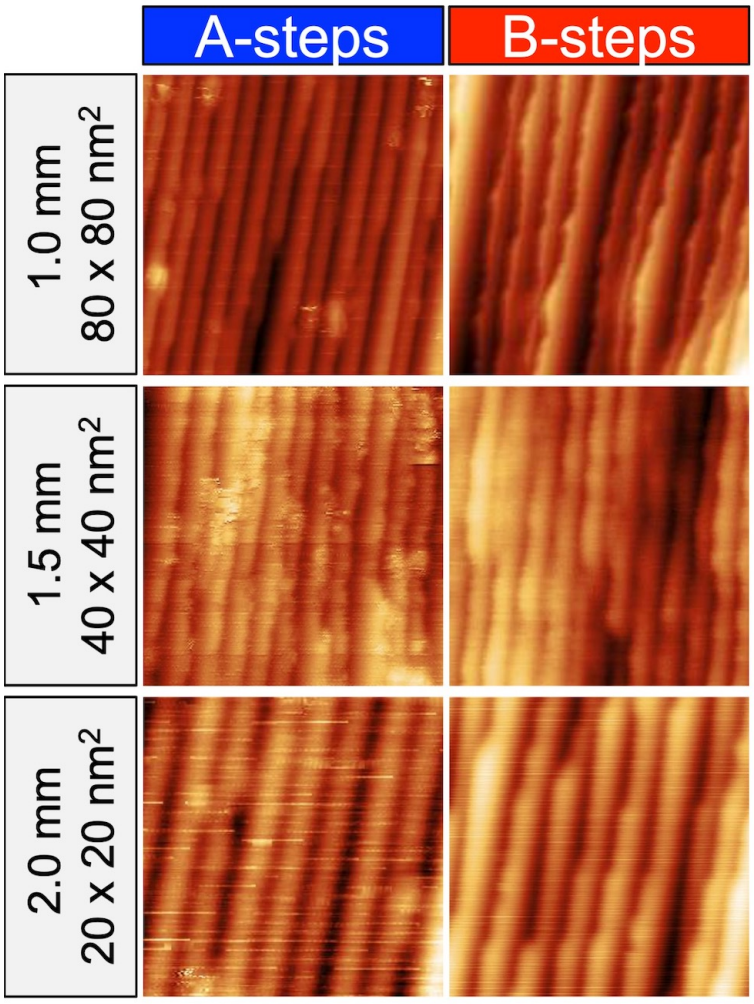

Figure 1: STM images of clean c-Ag(111), (left column) A-type step side of the crystal and (right column) B-type step side of the crystal. The location relative to the apex (x position, mm) and image size (nm^2) is noted to the left of the images. Imaging conditions are as follows: 1.0 A [560 mV, 400 pA] ; 1.5 A [450 mV, 400 pA] ; 2.0 A [440 mV, 370 pA] ; 1.0 B [400 mV, 400 pA] ; 1.5 B [500 mV, 400 pA] ; 2.0 B [400 mV, 400 pA]

similar results. Results are plotted in Figure 2 (circle markers) with error bars reflecting one standard deviation from multiple measurements. Also shown is the step density expected for the ideal bulk-trunctated surface (solid lines) determined using[41]

$$\rho_{step} = x \times \frac{\sqrt{3}}{r \times a} \tag{1}$$

where x is the displacement from the crystal apex, a is the bulk Ag lattice parameter (4.08 Å), and r is the radius of the sample (15 mm). The step heights were verified at various positions across the crystal. The average step height was $\approx$ 2.4 Å, in agreement with the literature.[47] Thus, our findings confirmed the applied cleaning procedures yielded a clean surface with a smooth step density variation for this curved Ag(111) crystal.

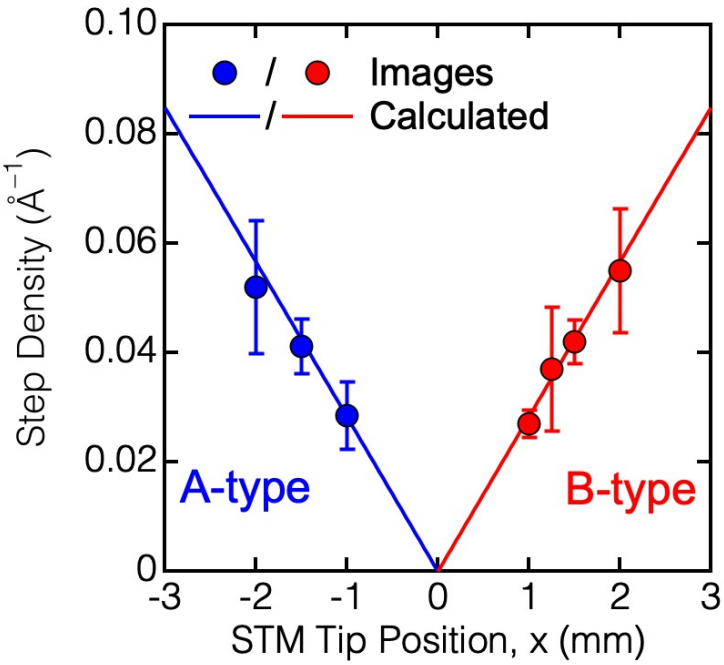

Figure 2: Experimentally determined step density, ρ_{step}, versus position along the curved surface as measured in mm from apex. Blue circles at negative values refer to A-type (100) steps and red circles at positive values refer to B-type (110) steps. The solid lines are the ideal step densities calculated from the crystal geometry.

The c-Ag(111) crystal surface was subsequently exposed to various amounts of atomic oxygen with the surface temperature (T_s) held at 525 K. The atomic oxygen source employed[48] yielded an O atom flux at the crystal surface of (1.2 $\pm$ 0.6) $\times$ 10^{-3} ML s^{-1} (ML

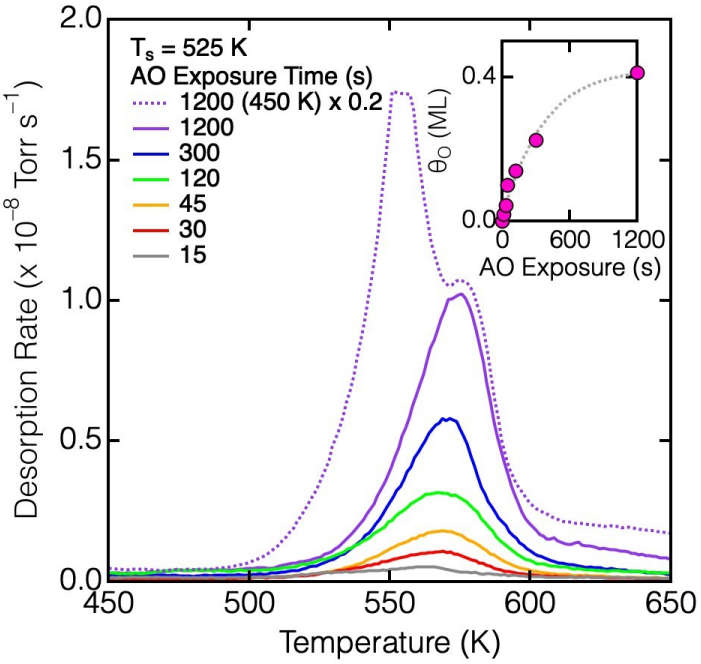

Figure 3: TPD spectra from *c*-Ag(111) after atomic oxygen exposures of varying duration. All spectra were obtained with a ramp rate of 3 K s^{-1}. Unless noted, all atomic oxygen exposures were at T_s = 525 K. Inset shows integrated desorption (θ_O) in ML versus atomic oxygen exposure time in seconds.

is defined with respect to Ag(111); 1 ML = 1.8×10^{15} Ag cm^{-2}). The flux was calculated assuming unity sticking probability at low θ_O. The Ir filament used for atomic oxygen dosing was positioned to evenly dose atomic oxygen across the entire crystal face. The uniform atomic oxygen flux at the crystal surface was verified using a planar Ag(111) crystal. We monitored the amount of O that stuck to the Ag(111) surface and found that it did not change by translating the crystal lengthwise ± 5 mm from the *c*-Ag(111) dosing position. Considering that the curved crystal surface was only 8 mm long and that we imaged the area ± 2 mm from the apex in this study, the atomic oxygen flux was uniform across the relevant part of the crystal face. After atomic oxygen exposure, the crystal was cooled to ≈ 35 K, STM images were obtained, and Temperature Programmed Desorption (TPD) spectra were taken. The latter were used to define the total uptake of atomic oxygen by the crystal by integration of the recombinative desorption peaks, and these spectra form the basis for the determination of the oxygen coverage. Figure 3 shows representative TPD spectra after several atomic oxygen exposures, and the inset shows the relationship between oxygen coverage (θ_O, in ML O) and atomic oxygen exposure time. The TPD spectral characteristics agreed with spectra from similar exposures on planar Ag(111).[16,22,45] After atomic oxygen exposure at T_s = 525 K, O_{ad} recombinatively desorbed in a TPD measurement as a single peak near 575 K. With increasing atomic oxygen exposure time, the peak area grew monotonically until 1200 s where $\theta_O \approx 0.4$ ML O, and O uptake ceased. As has been previously reported, the single TPD peak after atomic oxygen exposure at T_s = 525 K corresponds to a surface saturated with oxygen.[22] When T_s < 500 K, O_{sub} formed in parallel to the surface bound O species. The emergence of O_{sub} was characterized by the desorption peak at 550 K in Figure 3 (dashed purple trace). Note that the surface desorption peak at 575 K remained unchanged.[16,22] In summary, the characteristics of oxygen desorption were very similar for Ag(111) and *c*-Ag(111). The peak desorption temperature was unchanged and there were no additional desorption peaks in the TPD spectra as a result of the presence of A and B-type steps on the curved Ag(111) crystal.

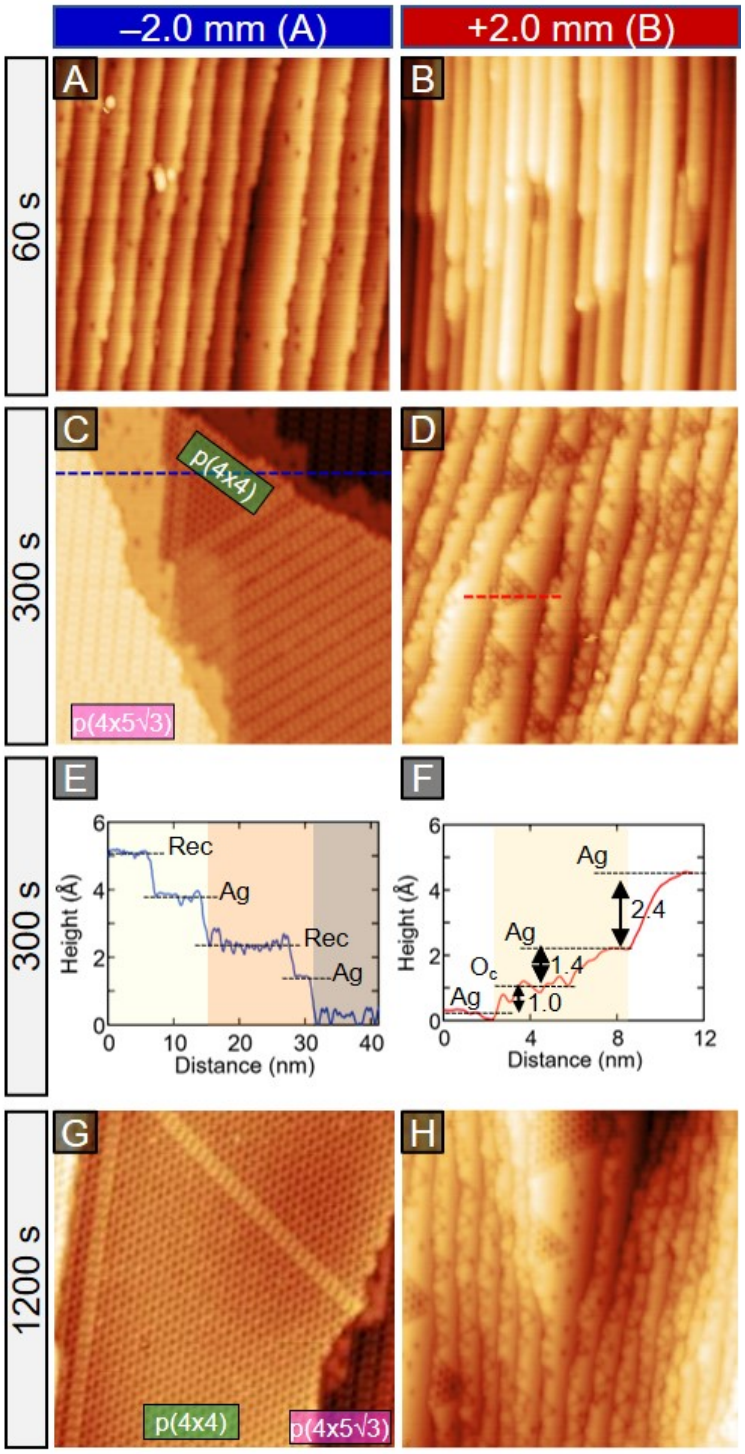

Figure 4: STM images obtained after different atomic oxygen exposures at both –2.0 mm (A) and +2.0 mm (B) on c-Ag(111). All images are 45 x 45 nm^2. Imaging conditions are: A) 500 mV, 400 pA; B) 400 mV, 400 pA; C) 480 mV, 460 pA; D) 600 mV, 490 pA; G) 400 mV, 460 pA; H) 440 mV, 460 pA. Panels E) and F) are the line profiles depicted in C) and D).

In contrast to the similarities between planar and curved Ag(111) TPD spectra, STM images clearly show that the local oxygen uptake and extent of reconstruction differed between the A and B-type step sides of the *c*-Ag(111) crystal. Figure 4 shows a series of representative STM images taken at −2.0 mm (A-type steps) and +2.0 mm (B-type steps). The average terrace width on the clean Ag surface at these positions corresponded to approximately 7 atomic rows of the (111) terrace. On the side with A-type steps, O uptake and reconstruction proceeded in a similar fashion to planar Ag(111).[11,22,23,45] Initially, we observed scattered chemisorbed O (O_c) atoms on the flat terraces (Figure 4A), and a roughly factor of two decrease in step density from the clean surface, while the steps remained 2.4 Å high. O_c appeared as dark depressions. With continued atomic oxygen exposure, the surface reconstructed into the $p(4 \times 5\sqrt{3})$ and $p(4 \times 4)$ reconstructions, as shown in Figure 4C. The reconstructions appeared elevated relative to neighboring Ag patches by approximately 1.0 Å. The contrast was as expected for the bias between STM tip and surface.[49,50] While some terraces were completely reconstructed, others were not. Where we observed remaining Ag patches with some O_c, the Ag step edges were straight and remained along the original direction of the clean stepped surface. Figure S1 provides a larger version of the same image with these edges marked. A line scan along the dashed blue line in Figure 4C is shown separately in Figure 4E. This shows the heights between Ag planes (2.4 Å) and the apparent elevation of the reconstructions (1.0 Å). These figures also illustrate how the step density decreased further upon oxidation. While Figure 4A shows approximately 12 steps, Figure 4C shows only 3 steps. After prolonged exposures, the surface was covered with domains of $p(4 \times 5\sqrt{3})$ and $p(4 \times 4)$ reconstructions. This is shown in Figures 4C and 4G. Formation of larger reconstructed areas repelled atomic steps. STM images suggested that the steps were conserved, possibly also resulting in nano-faceted areas. The steps likely migrated and bunched with the growth of reconstruction on the terraces. Figure S3 shows an STM image where the reconstruction planarization appeared to induce step bunching. Additional lines scans shown in Figure S2 illustrate that the apparent height between reconstructed planes

remained 2.4 Å.

We found a different development in the uptake of atomic oxygen and the formation of reconstructions on the B-type step side of the *c*-Ag(111) crystal. Representative images are shown in Figures 4B, 4D, and 4H. In contrast to Figure 4A, few O_c atoms were scattered on the (111) terraces after the 60 s exposure as shown in Figure 4B. After 300 s (Figure 4D) and 1200 s (Figure 4H) of atomic oxygen exposure, terraces were still largely clean with occasional small, dark triangular patches extending from a Ag step inward on the upper terrace. The included angle of these patches was 60°. Neither the contrast in these patches nor the structure were identical to the regularly observed silver reconstructions appearing in Figures 4C and 4G. Height profiles, as exemplified in Figure 4F, also show that these triangular patches appeared lower than the Ag terraces to which they belong. Hence, these patches were clusters of O_c rather than reconstructions. Furthermore, the step density was unchanged. As opposed to the A-type step side, where we found extensive reconstruction and loss of step density, the B-type steps persisted, even after 1200 s atomic oxygen exposure (Figure 4H). Now, some triangular areas with a $p(4 \times 4)$ reconstruction appeared, but not to the extent seen on the A-type steps. Additionally, the perimeter around the $p(4 \times 4)$ patches had inverted contrast, and individual O_c atoms remained on the otherwise clean terraces. The oxygen coverage clearly varied between the A and B-type step sides, as shown in Figures 5G and 5H. The B-type steps (Figure 5H) were largely non-reconstructed areas with only a small amount of O_c, while the A-type steps (Figure 5G) were extensively reconstructed.

The areal fractions of reconstructed areas (f_{rec}) on *c*-Ag(111) were obtained from STM images taken across the crystal after various atomic oxygen exposure durations. These data are plotted in Figure 5. At least 20 images were analyzed at each position. In Figure 5, the black trace shows the rapid development toward a fully reconstructed surface at the apex, and the reconstruction on the A and B-type step sides are shown by the blue and red markers, respectively. The solid circles represent ± 1.0 mm and the open circles represent ± 2.0 mm. Instead of plotting f_{rec} versus atomic oxygen exposure time, it was plotted with

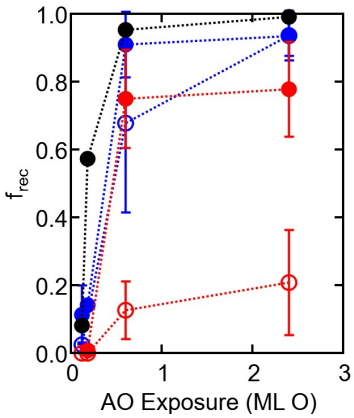

Figure 5: Areal fraction of O-induced reconstruction (with $\theta_O \approx 0.4$ ML) after atomic oxygen exposure at $T_s = 525$ K at various positions across the crystal face. A-type steps: open blue circles at -2.0 mm, solid blue circles at -1.0 mm. B-type steps: open red circles at +2.0 mm, solid red circles at +1.0 mm. (111) apex in black.

respect to atomic oxygen exposure in terms of ML O (atoms of O per surface Ag atom). In particular, the results suggest that areas with A-type steps developed reconstructions modestly slower than the (111) apex, but the difference between f_{rec} at the apex and on the A-type step side of the crystal was small. On the B-type step side, however, O uptake and reconstruction were considerably hindered. This effect seems related to the terrace width, as delayed reconstruction was prominent beyond +1.0 mm from the apex. The results in Figure 5 shows that oxidation of Ag(111) planes was kinetically controlled by step geometry, as O_c diffusion is rapid at 525 K. Terraces with average widths of several tens of Å and B-type step truncation resisted the incorporation of O and reconstruction of the topmost layer much more so than terraces truncated by A-type steps.

We are only able to speculate on the origin of the difference in oxidation. One possible explanation for a lower oxygen incorporation rate on the B-type step side of the crystal is that O_2 recombinative desorption was more efficient on B-type steps in comparison to A-type steps or (111) terrace sites. Such efficient competition with atomic oxygen adsorption would result in slower O accumulation during atomic oxygen exposure at $T_s = 525$ K. A significantly higher desorption rate at B-type steps would imply that O atoms bind less strongly to B-type steps than to terraces. A lower binding energy for O atoms at B-type

steps is, however, improbable because such behavior is inconsistent with observations and density functional theory (DFT) calculations for dissociation of O_2 at steps and kinks on a range of close-packed transition metal surfaces. The scaling relations generally hold, and O_{ad} are bound more strongly to sites with lower coordination than the (111) terrace sites.[51]

An alternative explanation for our observations takes not the level of oxygen coverage and reconstruction as the starting point, but the observed difference in retention of the step structure. On the A-type step side, planarization occurred in conjunction with the appearance of reconstructed areas, while on the B-type step side the step structure remained mostly intact. This suggests that the diffusivity of steps on the two sides of the crystal differed during atomic oxygen exposure and formation of reconstructions. On one hand, the free energies of clean A-type and B-type steps on Ag(111) are known to be nearly identical from calculation[52] and experiment,[53] and their diffusivity is already high at temperatures well below the T_s used here during atomic oxygen exposure.[54] On the other hand, pinning of steps by defects or impurties[55] as well as oxygen-induced faceting[56] has been documented on Ag(110). We believe the geometry of the nucleation sites is the key factor behind the observed difference.

Step structure retention (or lack thereof) may be traced by amount of oxidation as well as initial nucleation site of reconstruction formation. Loss of diffusivity of the B-type steps caused by the initial atomic oxygen oxidation would explain why the step structure in Figure 4D and 4H was retained. It also explains why O_c was found at low exposures on the (111) terraces with A-type steps, but not on the (111) terraces with B-type steps. Formation of silver oxide phases on Ag(111) requires significant reorganization and expansion of the lattice, both lateral and normal to the surface. From close examination of more than a dozen similar images, we found that the smaller oxidized patches were always along the top step edge on the B-type side, as illustrated by Figures 4D and 4F. Hence, on this side of the crystal, reconstructions originated from the top of B-type step edges. The line profile in Figure 4F illustrates that the limited oxidation bordering the step edge had not proceeded

all the way through to the end of the terrace. The step heights of the line profile depicted in Figure 4F show a step height between clean steps of 2.4 Å. The growth of the reconstruction on the step edges decreased the step height to 1.4 Å while initial oxidation simultaneously pinned the step in place. In summary, we find reason to believe that the B-type steps are immediately pinned by inital oxidation, and that the oxidized B-type step freezes the highly stepped structure, which opposes the required 'flexibility' for reconstruction. For rather narrow terraces, no variation in terrace width may occur once oxidized.

Scrutinizing images from the A-type step side of the crystal we found that the reconstruction patches consistently grew from the bottom of steps outward onto terraces, as determined by line profiling. Hence, while on the B-type step side formation of reconstructions may be hindered by pinning of steps by oxidation, on the A-type step side, formation of reconstruction traced the meandering metallic Ag step. These results are illustrated in Figure 4C, which depicts three steps corresponding to the three shaded regions of the line profiles in Figure 4E. The left (light yellow in the line profile) and middle (orange) steps were partially oxidized. The right (brown) step was fully reconstructed. A line profile across the top of Figure 4C depicts the height difference between the clean metal patches and reconstuction on the steps shown in Figure 4E in blue. The metal-metal step height was approximately 2.5 Å while the growth of reconstruction on the step diminishes the step height by about 1.0 Å. As the reconstruction grew on the terrace, the step edge meandered, allowing formation of large reconstructed areas seen on A-type steps. Once the step was fully reconstructed, it was pinned in place.

The nucleus of reconstruction formation on steps and terraces may have varied in location for the two types of step edge geometries and local Ag-O step structures. Clearly, our observations could also be a combination of differences between A and B-type steps, i.e. their rate of forming reconstructions, their recombinative desorption rates, and their diffusivity in both the clean and oxidized states. In any case, our results clearly demonstrate that the narrow B-type steps reduce oxygen-induced reconstruction.

The observation of increased uptake and reconstruction of oxygen on the A-type step side of the crystal indicated that the A-type step geometry was more reactive than the B-type step geometry. The geometry of the A-type steps reconstructed more when exposed to atomic oxygen when compared to the B-type steps under the same oxidizing conditions. Because the curved crystal had both A-type and B-type steps in a single sample, they were exposed to identical oxidizing conditions. Therefore, the step geometry alone dictated the amount of oxygen accumulation and fractional reconstruction on the crystal. Reconstruction was facile on terraces with A-type step geometries but not on terraces with B-type step geometries.

Conclusions

Oxygen-induced reconstruction and sticking was hindered on narrow Ag(111) terraces with B-type step geometry. On these terraces, atomic oxygen exposures yielded only small patches of reconstruction and low coverages of chemisorbed oxygen. Alternatively, on the A-type step side, the same exposures caused the terraces to readily reconstruct forming widened terraces. These findings are relevant to silver-catalyzed partial oxidation reactions as the step geometry hindered the formation of the undesirable nucleophilic oxygen bound up in surface reconstruction, and in principle, freed up more of the surface for the heterogeneously-catalyzed reaction.

Acknowledgement

We wish to acknowledge support from the National Science Foundation through award CHE-1800291. M.E. Turano thanks The Arthur J. Schmitt Foundation for support during this work. L.B.F. Juurlink thanks the EuroScolars Program for funding a visit to Loyola University Chicago to locally partake in the described experiments and research.

Supporting Information Available

Depiction of reconstruction growth in Figure 4C, line profiles of reconstruction height

References

(1) Schmid, M.; Reicho, A.; Stierle, A.; Costina, I.; Klikovits, J.; Kostelnik, P.; Dubay, O.; Kresse, G.; Gustafson, J.; Lundgren, E., et al. Structure of Ag (111)- p (4× 4)- O: no silver oxide. *Physical Review Letters* **2006**, *96*, 146102.

(2) Kleyn, A.; Butler, D.; Raukema, A. Dynamics of the interaction of O_2 with silver surfaces. *Surface Science* **1996**, *363*, 29–41.

(3) Rovida, G.; Pratesi, F.; Maglietta, M.; Ferroni, E. Effects of oxygen on silver surface structure. *Journal of Vacuum Science and Technology* **1972**, *9*, 796–799.

(4) Rovida, G.; Pratesi, F.; Maglietta, M.; Ferroni, E. Chemisorption of oxygen on the silver (111) surface. *Surface Science* **1974**, *43*, 230–256.

(5) Campbell, C. T. Atomic and molecular oxygen adsorption on Ag (111). *Surface Science* **1985**, *157*, 43–60.

(6) Schnadt, J.; Michaelides, A.; Knudsen, J.; Vang, R. T.; Reuter, K.; Lægsgaard, E.; Scheffler, M.; Besenbacher, F. Revisiting the structure of the p (4× 4) surface oxide on Ag (111). *Physical Review Letters* **2006**, *96*, 146101.

(7) LeFort, T. E. Process for the production of ethylene oxide. Patent US600578A, 1935.

(8) Le Blanc, M.; Plaschke, E. Über die darstellung von formaldehyd aus methylalkohol nach dem kontaktverfahren. *Zeitschrift für Elektrochemie und Angewandte Physikalische Chemie* **1911**, *17*, 45–57.

(9) Böcklein, S.; Günther, S.; Wintterlin, J. High-Pressure scanning tunneling microscopy of a silver surface during catalytic formation of ethylene oxide. *Angewandte Chemie International Edition* **2013**, *52*, 5518–5521.

(10) Chen, B. W.; Kirvassilis, D.; Bai, Y.; Mavrikakis, M. Atomic and molecular adsorption on Ag (111). *The Journal of Physical Chemistry C* **2018**, *123*, 7551–7566.

(11) Martin, N.; Klacar, S.; Gronbeck, H.; Knudsen, J.; Schnadt, J.; Blomberg, S.; Gustafson, J.; Lundgren, E. High-coverage oxygen-induced surface structures on Ag (111). *The Journal of Physical Chemistry C* **2014**, *118*, 15324–15331.

(12) Pu, T.; Tian, H.; Ford, M. E.; Rangarajan, S.; Wachs, I. E. Overview of selective oxidation of ethylene to ethylene oxide by Ag catalysts. *ACS Catalysis* **2019**, *9*, 10727–10750.

(13) Kenge, N.; Pitale, S.; Joshi, K. The nature of electrophilic oxygen: insights from periodic density functional theory investigations. *Surface Science* **2019**, *679*, 188–195.

(14) Jones, T. E.; Wyrwich, R.; Bocklein, S.; Carbonio, E. A.; Greiner, M. T.; Klyushin, A. Y.; Moritz, W.; Locatelli, A.; Mentes, T. O.; Nino, M. A., et al. The selective species in ethylene epoxidation on silver. *ACS Catalysis* **2018**, *8*, 3844–3852.

(15) Özbek, M.; Van Santen, R. The mechanism of ethylene epoxidation catalysis. *Catalysis Letters* **2013**, *143*, 131–141.

(16) Turano, M. E.; Farber, R. G.; Oskorep, E. C.; Rosenberg, R. A.; Killelea, D. R. Characterization of oxygenaceous species formed by exposure of Ag (111) to atomic oxygen. *The Journal of Physical Chemistry C* **2019**, *124*, 1382–1389.

(17) Lamoth, M.; Jones, T.; Plodinec, M.; Machoke, A.; Wrabetz, S.; Krämer, M.; Karpov, A.; Rosowski, F.; Piccinin, S.; Schlögl, R., et al. Nanocatalysts unravel the selective state of Ag. *ChemCatChem* **2020**, *12*, 2977–2988.

(18) Hus, M.; Hellman, A. Ethylene epoxidation on Ag (100), Ag (110), and Ag (111): a joint ab initio and kinetic monte carlo study and comparison with experiments. *ACS Catalysis* **2018**, *9*, 1183–1196.

(19) Özbek, M. O.; Önal, I.; van Santen, R. A. Chlorine and caesium promotion of silver ethylene epoxidation catalysts. *ChemCatChem* **2013**, *5*, 443–451.

(20) Günther, S.; Böcklein, S.; Wintterlin, J.; Niño, M. A.; Menteş, T. O.; Locatelli, A. Locating catalytically active oxygen on Ag (1 1 1)—A spectromicroscopy study. *ChemCatChem* **2013**, *5*, 3342–3350.

(21) Rocha, T. C. R.; Oestereich, A.; Demidov, D. V.; Havecker, M.; Zafeiratos, S.; Weinberg, G.; Bukhtiyarov, V. I.; Knop-Gericke, A.; Schlögl, R. The silver-oxygen system in catalysis: new insights by near ambient pressure X-ray photoelectron spectroscopy. *Physical Chemistry Chemical Physics* **2012**, *14*, 4554–4564.

(22) Derouin, J.; Farber, R. G.; Turano, M. E.; Iski, E. V.; Killelea, D. R. Thermally selective formation of subsurface oxygen in Ag (111) and consequent surface structure. *ACS Catalysis* **2016**, *6*, 4640–4646.

(23) Schnadt, J.; Knudsen, J.; Hu, X. L.; Michaelides, A.; Vang, R. T.; Reuter, K.; Li, Z.; Lægsgaard, E.; Scheffler, M.; Besenbacher, F. Experimental and theoretical study of oxygen adsorption structures on Ag (111). *Physical Review B* **2009**, *80*, 075424.

(24) Carbonio, E. A.; Rocha, T. C.; Klyushin, A. Y.; Píš, I.; Magnano, E.; Nappini, S.; Piccinin, S.; Knop-Gericke, A.; Schlögl, R.; Jones, T. E. Are multiple oxygen species selective in ethylene epoxidation on silver? *Chemical Science* **2018**, *9*, 990–998.

(25) Jones, T. E.; Rocha, T. C.; Knop-Gericke, A.; Stampfl, C.; Schlögl, R.; Piccinin, S. Insights into the electronic structure of the oxygen species active in alkene epoxidation on silver. *ACS Catalysis* **2015**, *5*, 5846–5850.

(26) Xia, Y.; Xiong, Y.; Lim, B.; Skrabalak, S. E. Shape-controlled synthesis of metal nanocrystals: simple chemistry meets complex physics? *Angewandte Chemie International Edition* **2009**, *48*, 60–103.

(27) Wiley, B.; Sun, Y.; Xia, Y. Synthesis of silver nanostructures with controlled shapes and properties. *Accounts of Chemical Research* **2007**, *40*, 1067–1076.

(28) Cipriani, G.; Loffreda, D.; Dal Corso, A.; de Gironcoli, S.; Baroni, S. Adsorption of atomic oxygen on Ag (001): a study based on density-functional theory. *Surface Science* **2002**, *501*, 182–190.

(29) Fang, C. A. Surface structural transition of adsorption of oxygen on Ag (100). *Surface Science* **1990**, *235*, L291–L294.

(30) Balmes, O.; Prévot, G.; Torrelles, X.; Lundgren, E.; Ferrer, S. Diatomic steps in Pt (997) surfaces are better catalysts than monatomic steps for the CO oxidation reaction near atmospheric pressure. *ACS Catalysis* **2016**, *6*, 1285–1291.

(31) Garcia-Martinez, F.; Schiller, F.; Blomberg, S.; Shipilin, M.; Merte, L. R.; Gustafson, J.; Lundgren, E.; Ortega, J. E. CO chemisorption on vicinal Rh (111) surfaces studied with a curved crystal. *The Journal of Physical Chemistry C* **2020**, *124*, 9305–9313.

(32) Somorjai, G. A.; York, R. L.; Butcher, D.; Park, J. Y. The evolution of model catalytic systems; studies of structure, bonding and dynamics from single crystal metal surfaces to nanoparticles, and from low pressure ($<10^{-3}$ Torr) to high pressure ($>10^{-3}$ Torr) to liquid interfaces. *Physical Chemistry Chemical Physics* **2007**, *9*, 3500–3513.

(33) Zhu, Q.; Saidi, W. A.; Yang, J. C. Step-edge directed metal oxidation. *The Journal of Physical Chemistry Letters* **2016**, *7*, 2530–2536.

(34) Goodman, D. W. Correlations between surface science models and "real-world" catalysts. *The Journal of Physical Chemistry* **1996**, *100*, 13090–13102.

(35) Savio, L.; Vattuone, L.; Rocca, M. From adsorption at the surface to incorporation into subsurface sites: the role of steps for O/Ag. *Applied Physics A* **2007**, *87*, 399–404.

(36) De Mongeot, F. B.; Cupolillo, A.; Valbusa, U.; Rocca, M. O_2 dissociation on Ag (001): the role of kink sites. *Chemical Physics Letters* **1997**, *270*, 345–350.

(37) van Lent, R.; Auras, S. V.; Cao, K.; Walsh, A. J.; Gleeson, M. A.; Juurlink, L. B. F. Site-specific reactivity of molecules with surface defects—the case of H_2 dissociation on Pt. *Science* **2019**, *363*, 155–157.

(38) Walsh, A. J.; van Lent, R.; Auras, S. V.; Gleeson, M. A.; Berg, O. T.; Juurlink, L. B. F. Step-type and step-density influences on CO adsorption probed by reflection absorption infrared spectroscopy using a curved Pt (111) surface. *Journal of Vacuum Science & Technology A: Vacuum, Surfaces, and Films* **2017**, *35*, 03E102.

(39) Lawton, T.; Pushkarev, V.; Broitman, E.; Reinicker, A.; Sykes, E.; Gellman, A. Initial oxidation of Cu (hkl) surfaces vicinal to Cu (111): a high-throughput study of structure sensitivity. *The Journal of Physical Chemistry C* **2012**, *116*, 16054–16062.

(40) Walter, A. L.; Schiller, F.; Corso, M.; Merte, L. R.; Bertram, F.; Lobo-Checa, J.; Shipilin, M.; Gustafson, J.; Lundgren, E.; Brión-Ríos, A. X., et al. X-ray photoemission analysis of clean and carbon monoxide-chemisorbed platinum (111) stepped surfaces using a curved crystal. *Nature Communications* **2015**, *6*, 1–7.

(41) Auras, S. V.; Juurlink, L. B. F. Recent advances in the use of curved single crystal surfaces. *Progress in Surface Science* **2021**, *96*, 100627.

(42) Auras, S. V.; van Bree, R. A.; Bashlakov, D. L.; van Lent, R.; Juurlink, L. B. F. It's not just the defects–a curved crystal study of H_2O desorption from Ag. *Physical Chemistry Chemical Physics* **2019**, *21*, 15422–15430.

(43) Janlamool, J.; Bashlakov, D.; Berg, O.; Praserthdam, P.; Jongsomjit, B.; Juurlink, L. B. F. Desorption of water from distinct step types on a curved silver crystal. *Molecules* **2014**, *19*, 10845–10862.

(44) Ortega, J. E.; Corso, M.; Abd-el Fattah, Z.; Goiri, E.; Schiller, F. Interplay between structure and electronic states in step arrays explored with curved surfaces. *Physical Review B* **2011**, *83*, 085411.

(45) Derouin, J.; Farber, R.; Heslop, S.; Killelea, D. Formation of surface oxides and Ag_2O thin films with atomic oxygen on Ag(111). *Surface Science* **2015**, *641*, L1–4.

(46) Umemoto, H.; Kusanagi, H. Catalytic decomposition of O_2, NO, N_2O, and NO_2 on a heated Ir filament to produce atomic oxygen. *Journal of Physics D: Applied Physics* **2008**, *41*, 225505.

(47) Ortega, J. E.; Vasseur, G.; Piquero-Zulaica, I.; Matencio, S.; Valbuena, M. A.; Rault, J. E.; Schiller, F.; Corso, M.; Mugarza, A.; Lobo-Checa, J. Structure and electronic states of vicinal Ag (111) surfaces with densely kinked steps. *New Journal of Physics* **2018**, *20*, 073010.

(48) Derouin, J.; Farber, R.; Killelea, D. Combined STM and TPD study of Rh(111) under conditions of high oxygen coverage. *The Journal of Physical Chemistry C* **2015**, *119*, 14748–14755.

(49) Carlisle, C.; Fujimoto, T.; Sim, W.; King, D. Atomic imaging of the transition between oxygen chemisorption and oxide film growth on Ag(111). *Surface Science* **2000**, *470*, 15–31.

(50) Baber, A.; Xu, F.; Dvorak, F.; Mudiyanselage, K.; Soldemo, M.; Weissenrieder, J.; Senanayake, S.; Sadowski, J.; Rodriguez, J.; Matolín, V., et al. In situ imaging of Cu_2O under reducing conditions: formation of metallic fronts by mass transfer. *The Journal of the American Chemical Society* **2013**, *135*, 16781–16784.

(51) Jiang, T.; Mowbray, D.; Dobrin, S.; Falsig, H.; Hvolbæk, B.; Bligaard, T.; Nørskov, J. K. Trends in CO oxidation rates for metal nanoparticles and close-packed, stepped, and kinked surfaces. *The Journal of Physical Chemistry C* **2009**, *113*, 10548–10553.

(52) Nelson, R.; Einstein, T.; Khare, S.; Rous, P. Energies of steps, kinks, and defects on Ag {100} and Ag {111} using the embedded atom method, and some consequences. *Surface Science* **1993**, *295*, 462–484.

(53) Morgenstern, K.; Rosenfeld, G.; Comsa, G. Decay of two-dimensional Ag islands on Ag (111). *Physical Review Letters* **1996**, *76*, 2113.

(54) Poensgen, M.; Wolf, J.; Frohn, J.; Giesen, M.; Ibach, H. Step dynamics on Ag (111) and Cu (100) surfaces. *Surface Science* **1992**, *274*, 430–440.

(55) Ozcomert, J.; Pai, W.; Bartelt, N.; Reutt-Robey, I. Step configurations near pinning sites on Ag (110). *Surface Science* **1993**, *293*, 183–194.

(56) Ozcomert, J.; Pai, W.; Bartelt, N.; Reutt-Robey, J. Kinetics of oxygen-induced faceting of vicinal Ag (110). *Physical Review Letters* **1994**, *72*, 258.

Graphical TOC Entry